AUT Journal of Civil Engineering

AUT J. Civil Eng., 6(1) (2022) 35-50
DOI: 10.22060/ajce.2022.20088.5757

Optimization of Tunnel Reinforcements by Genetic Algorithm with the Aim of Replacing with Fibers

M. H. Taghavi Parsa[1]*, H. Sharifi[2], P. Amirchoupani[3]

[1] Civil Group, University of Qom, Qom, Iran.
[2] Esfahan University, Esfahan, Iran.
[3] Faculty of Civil Engineering, Babol Noshirvani University of Technology, Babol, Iran.

ABSTRACT: In this study, the replacement of fibers with reinforcements of tunnel-reinforced concrete segments has been optimized using the method of the genetic algorithm by five fibers of steel, carbon, aramid, glass, and polypropylene, respectively. As an example, two steps of optimization of the Tehran metro, line seven, have been studied for this purpose. In the first step, the appropriate geometry is selected for the arrangement of the optimized ring reinforcements. The results showed a 62% removal of reinforcements. In the second step, the separated optimal percentages of all five types of fibers and the combination of steel fibers and polypropylene are expressed. Also, for a more accurate simulation of modeling the plastic part of the segment, the results of two methods have been validated, including CDP (concrete damage plasticity) and Brittle Cracking. According to the genetic algorithm, the optimized percentage for steel fibers is 1%, aramid fibers 3%, glass fibers 3%, carbon 1.1%, polypropylene 0.2%, and the composition of steel fibers 1% with 0.1 polypropylene is determined, as well.

Review History:

Received: May, 26, 2021
Revised: Apr. 16, 2022
Accepted: May, 07, 2022
Available Online: Jun. 22, 2022

Keywords:

Optimization
Genetic algorithm
Tunnel
Fiber concrete

1- Introduction

Tunnels are underground structures that are drilled for ease of transportation. After a long history of tunneling, tunnels with reinforced or unreinforced prefabricated concrete segments have become common in the last century. The replacement of bars with steel and non-steel fibers became more significant in tunnel concrete segments due to the executive difficulties and increase in tensile strength. Fiber-reinforced concrete structures were developed extensively in the last century due to the increase in tensile and compressive strength, toughness, durability, and decrease in the drop, resistance to wear and corrosion, etc. Fiber-reinforced concrete can improve many functions in tunnel cover. Hence, many tunnels have been constructed by using fiber-reinforced concrete segments in recent years. Today, the performance of tunnels against various loads has been improved by using steel fibers along with four fibers of carbon, aramid, glass, and polypropylene. The ACI544_7R [1] and ACI544_8R [2] are widely used to help the optimization of steel fiber tunnel reinforcement. The study of RILEM TC 162-TDF [3] and [4] Model Code 2010 regulations is also recommended for fiber-reinforced concrete segments. The widespread use of fiber-reinforced concrete with steel fibers (SFRC) has been common in the world since 1970. The main reason for using fibers in concrete is to control concrete cracks and delay the formation of primary concrete cracks. In 1994, Moysen *et al.* [5] developed the use of steel fibers in tunnels as a new research method. They compared plain concrete and steel fiber reinforced concrete and concluded that the addition of steel fiber increased the bending capacity of tunnel concrete. Also, the combination of steel fibers and reinforcement gives the best results in improving the bending performance and axial forces. In 2009, Chiaia *et al.* [6] studied the combined use of reinforcement and steel fibers in an integrated manner (not as a prefabricated tunnel). By examining the underground tunnel in Italy, they concluded that the excessive increase of steel fibers, along with the significant reduction of concrete cracks, caused the reinforcement and concrete to slip, which reduced the tensile strength of reinforced concrete. In 2011, Molins [7] conducted a numerical and experimental study of composite segments of reinforcement and steel fibers. They performed their experiments on real rings and loaded 15 life-size ring tunnels. They conducted real tests on the rings and placed 15 true-size rings under load. Then, the results were compared with experimental data. In the same year, Fuente *et al.* [8] increased the percentage of optimal reinforcement to 38% by adding 25 kg / m2 of steel fibers and verifying the numerical results obtained from ABACUS software in the laboratory. In 2014, Tiberti *et al.* [9] numerically optimized the tunnel of all the old reinforcement for steel fiber reinforcement. They modeled and simulated an old tunnel built with reinforcement, leaving only reinforcements close to the ground in the ring

*Corresponding author's email: dr.mhparsa@gmail.com

unchanged. Then, more than 50% of the upper and side reinforcements of the tunnel were removed and compensated with metal fibers. In 2014, Li *et al.* [10] optimized reinforced concrete slabs with carbon fiber-reinforced polymers using the numerical density method and topology optimization. They reduced and optimized concrete slab reinforcements based on increasing the load-bearing capacity by carbon fiber design. Also, their method for optimizing other concrete structures with reinforcement can be generalized. In 2016, Carmona *et al.* [11] examined the Barcelona 9 line for laboratory research into the actual distribution of steel fibers in the segment. The results showed that the accumulation of fibers in the corners and the lower surface of the arch is more than in the middle and upper surfaces of the arch. In 2017, Meng *et al.* [12] examined the connections of tunnel segments. They concluded that the flexural strength of segments made of steel fibers is higher than purely reinforced specimens. They also found that the initial crack appeared much earlier in all samples reinforced by steel bars. Cartley *et al.* [13] proposed the use of glass reinforcement instead of steel in tunnel prefabricated segments. The advantage of the mentioned reinforcements is the increase in corrosion resistance compared to steel reinforcements, which are also suitable for making dielectric connections. The most significant issue in this study is the increase in the estimated economic costs compared to steel reinforcement. In 2020, Al-Wasabi *et al.* [14] investigated the impact strength of a mixture of steel fibers and polypropylene. In this study, concrete specimens were subjected to a slow hammer fall test. They found that concrete made of 0.9% polypropylene fibers and 0.1% steel fibers increased the impact strength of concrete tenfold compared to plain concrete. They also concluded that with the increase of concrete particles, the impact resistance of concrete increases, and the compressive and tensile strength of fiber-reinforced concrete decreases. In 2020, Tengilimoglu *et al.* [15] investigated the effect of synthetic fibers and polypropylene along with tunnel segment reinforcements on a real scale. By constructing 14 tunnel segments made of synthetic fibers and polypropylene, they found that polypropylene fibers, although capable of splitting and controlling tensile stresses, were not able to control flexural stresses properly if used alone and without reinforcement. They found that if synthetic fibers were used in combination with polypropylene fibers, better results could be obtained than in the case of reinforcement and polypropylene fibers in the form of only flexural stresses. In 2020, Guo *et al.* [16] investigated carbon fiber-reinforced concrete at high temperatures. Additionally, Vivas *et al.* [17] investigated the impact strength of concrete made of glass, polypropylene, and metal fibers separately. They found that there was a relationship between static residual stresses and impact strength in concrete.

In this research, seven different mixing designs have been made for concrete by changing the length of carbon fibers and the volume percentage of fibers. The results show that the addition of carbon fiber at high temperatures increases the flexural strength of concrete while having a limited effect on the compressive strength of concrete. The results of this study showed that the small cracks of glass fibers, the large cracks of polypropylene fibers, and the pre-and post-cracking recovery in concrete steel fibers have shown better performance. In this research, with the help of a genetic algorithm and simulation in ABACUS, 62% of tunnel segment reinforcements have been removed and replaced.

2- Genetic Algorithm Optimization

The task of the optimization module in the ABACUS is to optimize the geometry of the structure to reduce materials and reduce costs [18]. The mechanism of the genetic algorithm is that a set of response points in each iteration moves toward the optimal solution. This answer is not necessarily the best possible answer, but the process of the algorithm converges toward superior answers. The completion of the algorithm is also defined either by defining the number of selected cycles or continuing the cycle until convergence is achieved in the results. In this study, first, according to ACI544-7R regulations and reputable scientific authorities to remove reinforcement that does not withstand high flexural and tensile stresses by the roulette cycle in the genetic algorithm, the chances of areas that are less involved with tunnel loads are lower and they are considered the delete option is included in the algorithm. On the other hand, the chances of segmental side reinforcements are defined in such a way that the initial population of the genetic algorithm is selected more than these areas. This part of the process optimization of geometry defined segment. Superior geometry is the geometry that has the most reduction of the reinforcement and also the final interaction curve of the ring is within the allowable range of ACI544-7R [1]. According to the mentioned condition, two geometries have been selected for the arrangement of the reinforcements, which represent the elimination of 62% and 70% of the segment reinforcements. Then, five steel fibers, glass, aramid, carbon, and polypropylene, which are resistant to tensile and flexural stresses, have been used to compensate for the removal effects of the reinforcement. Hence, the volume percentage of all fibers from zero to three percent with steps of 0.1 percent is considered. Therefore, for each fiber, there are 30 selected chances. The algorithm considers zero percent volume fibers and compares the interaction curve created by the optimal segment with the ACI544-7R code. If the interaction diagram is not within the regulations, one-tenth of a percent could increase the volume percentage of the fibers until the interaction curve is within the allowable range. For the combined state of polypropylene and steel fibers, the lowest volume percentage is considered for these two fibers. Hence, the interaction curve of the fabricated ring is within the allowable range of ACI544-7R. In addition to the chance of selecting fibers, there is also the chance of selecting superior geometry, which together makes up the initial population of the genetic algorithm of the present study. For example, in the fiber combination mode, the algorithm selects a geometry and then randomly selects two percent of the volume of the two fibers. Then, it examines the condition for checking the interaction curve with ACI544-

7R. If not allowed, the next geometric arrangement and a different volume percentage (between zero and three percent) are selected for both fibers. This chromosome (chance of selection) is selected if it is within the allowable range. This cycle is done until 6 parents are created. Now that the initial population is formed, randomly selected parents give birth. In this way, two parents from the initially selected population randomly transfer some of their characteristics to the child. The offspring have a geometric arrangement of reinforcement and the percentage of fibers selected by their parents at random. The permissibility of the children's interaction curve is then compared with ACI544-7R. This cycle will continue until the 6 accepted children are identified. Finally, some of the characteristics of the selected children are mutated and changed. This cycle also continues until the selection of 6 allowed chromosomes. The lowest percentage of composite fibers that can be within the allowable range of the interaction curve of ACI544-7R is known as the superior chromosome. To take a closer look at the research process, a flowchart of Fig. 1 is drawn, which includes the steps and operators mentioned.

3- Methods of operation

3- 1- Fiber Examination

A) Steel fibers: The high strength and modulus of the steel because these fibers have a good performance against impact loads. The tensile strength of steel is estimated at 345 to 2100 MPa. The only significant weakness of steel fibers is the possibility of corrosion. Due to the alkaline environment of the cement matrix and the use of stainless steel, this problem can be solved. The strength of these fibers against bending is also acceptable according to standard tests.

B) Glass fibers: The most famous common glass fibers used in concrete can be seven types: A-Glass, S-Glass, E-Glass, R-Glass, Z-Glass, D-Glass, and AR-Glass. Among these fibers, the E-Glass type with a tensile strength of about 350 MPa and Young modulus of about 5.72 GPa, and the S-Glass type, with a tensile strength of about 33.1 times that of the E-Glass type and Yang modulus of about 96 GPa, have the most applications in concrete.

C) Polypropylene fibers: Polypropylene (PP) fibers are not suitable for use alone in concrete against various loads due to their melting point and low modulus of elasticity. However, the combination of a small percentage of polypropylene fibers with steel fibers has reported satisfactory results. The advantages of these fibers include high resistance in acidic and alkaline environments.

D) Aramid fibers (a special type of nylon fiber): Aramid fibers have the brands Kevlar and Nomex. The advantages of these fibers include high heat resistance and high strength of these fibers. Also, the modulus of elasticity of these fibers in the direction of the fiber axis is very high. Disadvantages of these fibers include their low shear modulus.

E) Carbon fiber: The advantages of carbon fiber include high Young modulus (up to about 700 GPa), high thermal resistance, low weight, and high resistance in an alkaline environment. An important point in carbon fibers is the high cost of these fibers compared to the other fibers.

The mechanical properties of steel, glass, polypropylene, aramid, and carbon fibers are compared in Table 1, one by one [19-24].

Two important parameters for selecting fibers in concrete according to ASTM A820 [21] are high tensile and flexural strength. For this reason, these fibers have been selected for use in tunnel rings.

3- 2- Investigation of the concrete plastic part simulation method

In this study, a tunnel segment designed in ACI544-7R is drawn in a laboratory and modeled in ABAQUS software for validation. After applying different modules, the force-displacement curve between the segments is compared with numerical work. The designed segment is the work of Gettu *et al.* [23], who in 2004 placed the Barcelona Line 9 segment in the form of all-metal fibers with complete removal of reinforcement under a three-point bending test. This segment is a 48-degree segment of the 9th line of Barcelona, 7.4 meters long and 8.1 meters wide, which is 0.35 meters thick. In the simulation of the present study, the displacement-control method has been used to obtain the necessary force. Both CDP (concrete damage plasticity) and Brittle Cracking have been used to examine the force-displacement curve as closely as possible to assign plasticity properties. In CDP the force-displacement curve of the drop section is not shown because the elements are not removed, but in the Brittle cracking model, the drop section is also modeled. The advantage of the CDP model is that it applies to the application of soil geostatic stresses. The simulation images of this section are shown in Fig 2.

The force-displacement output for the model simulated by the CDP method and the model simulated by the Brittle Cracking model is shown in Fig 3. As shown in Fig. 3, in the Brittle Cracking model, the final drop section of the diagram is also consistent with the Gettu laboratory work. In the CDP model, it is not compatible with the laboratory work of the Gettu because it does not remove the corroded elements of the drop section. As illustrated in Fig. 3, to compare and evaluate the accuracy of results obtained from the present simulation with reference [24], the results obtained from the force-displacement curve in two CDP and Brittle Cracking models, are plotted with the results of the Gettu work.

As shown in Fig. 3, the CDP model failed to validate properly with the reference experimental work [23], but in the Brittle cracking model, the maximum tolerable load of the segment and the maximum displacement obtained are close to the laboratory results. The results of the two simulated models with the reference are compared in Table 2 [23].

According to Table 2, in the Brittle cracking model, the total error rate is 5%. Considering that the reference [23] is experimental research and the present simulation is numerical and has been examined from two different analyses of this segment and in the Brittle cracking model, like the experimental results, the drop section of the graph has been simulated, it seems that the obtained results can be cited. In

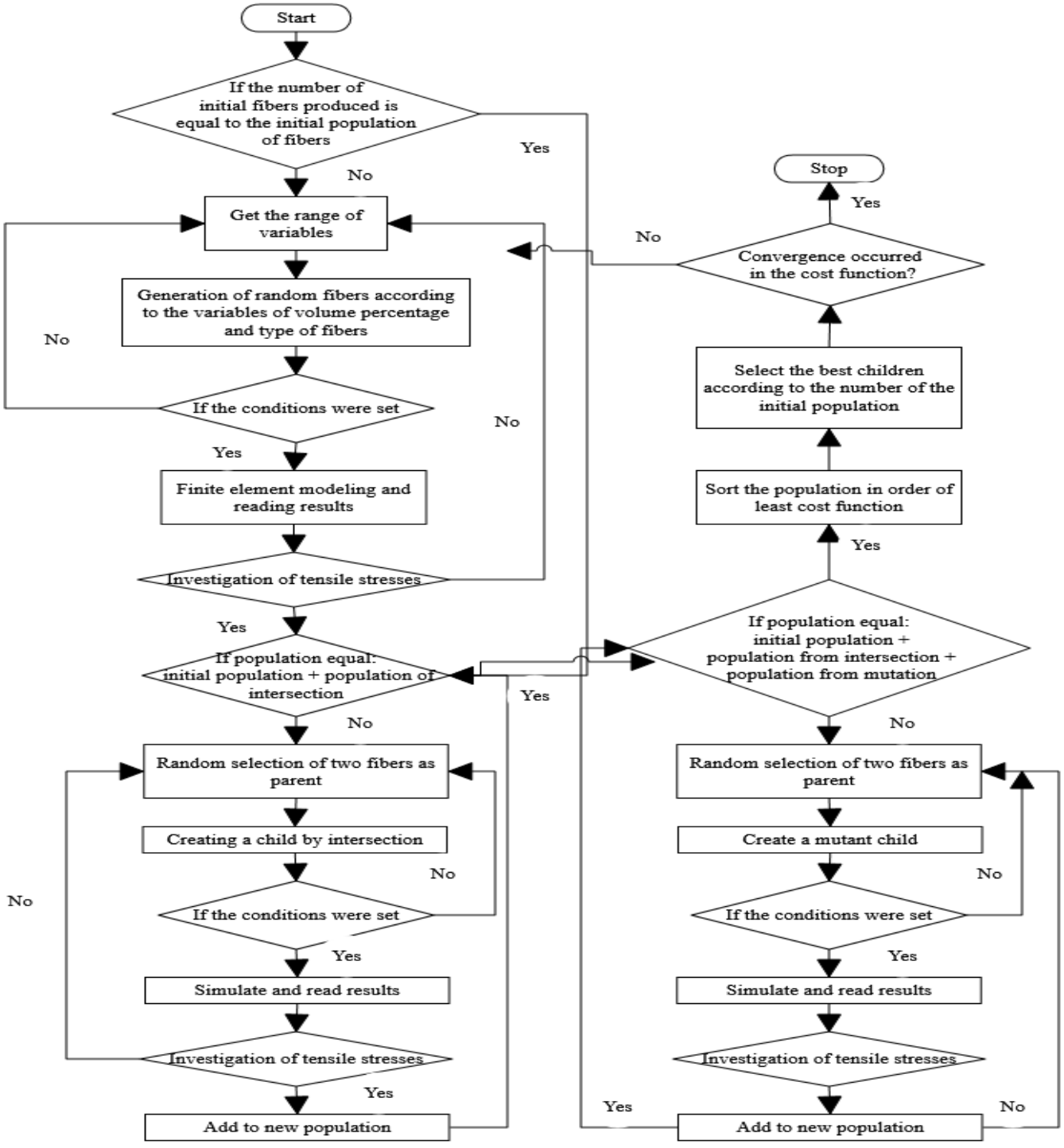

Fig. 1. Flowchart of genetic algorithm aimed at reducing armature.

Table 1. Comparison of mechanical properties of fibers [19-25].

Fiber properties	Tensile strength (GPa)	Modulus of elasticity (GPa)	Poisson's ratio	Specific density	Diameter (micrometers)	Elongation
Steel	0.5-2	200	0.28	7.84	5-500	0.5-3.5
Glass	2-4	70-80	0.22-0.25	2.6	9-15	2-3.5
Polypropylene	0.45-0.76	3.5-10	0.29-0.46	0.9-0.95	20-400	15-25
Aramid	2.3-3.5	63-120	0.32	1.44	10-12	2-4.5
Carbon	2.5-4	230-380	0.35	1.6-1.7	8-9	0.5-1.5

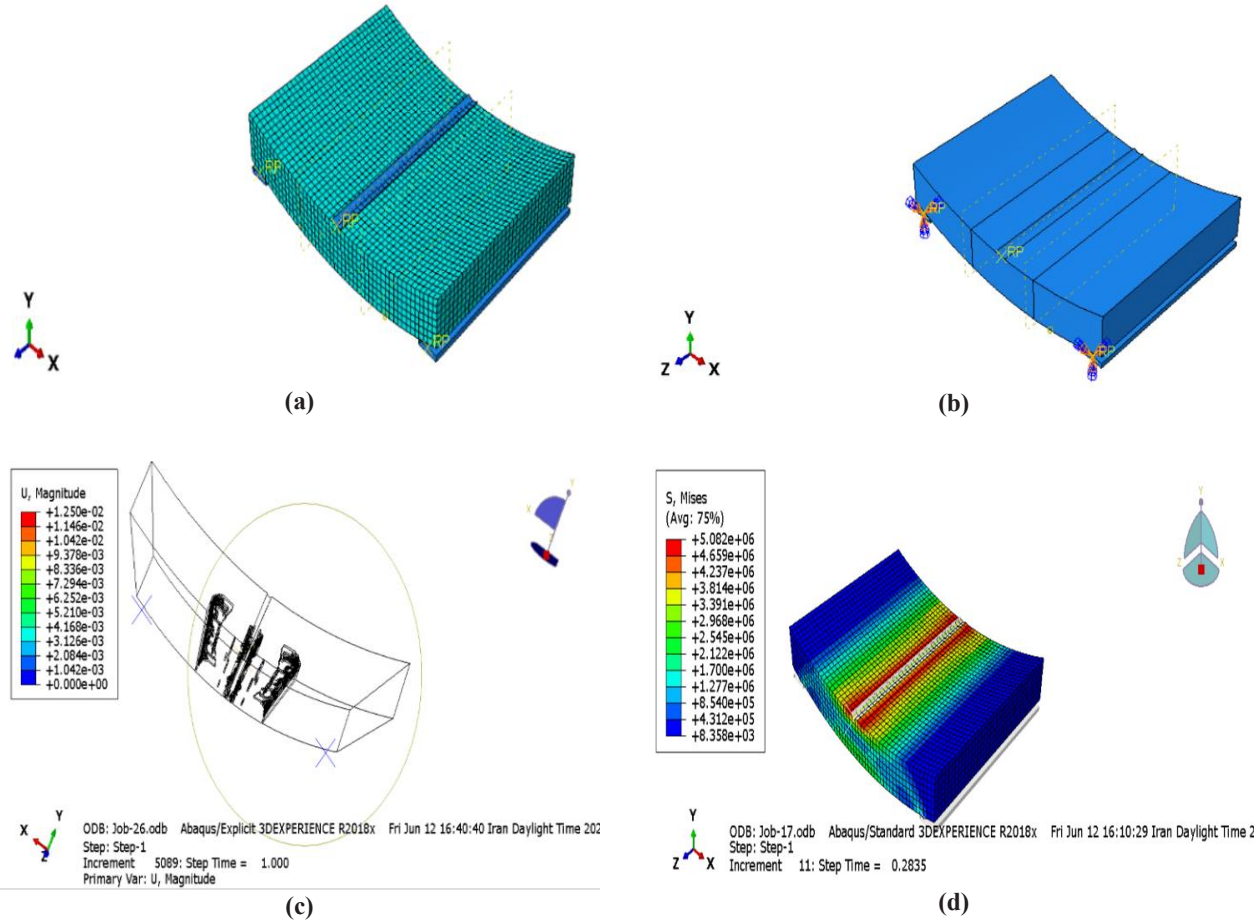

Fig. 2. Barcelona 9th line segment simulation a) Mesh generation b) Boundary conditions c) brittle cracking model d) output image.

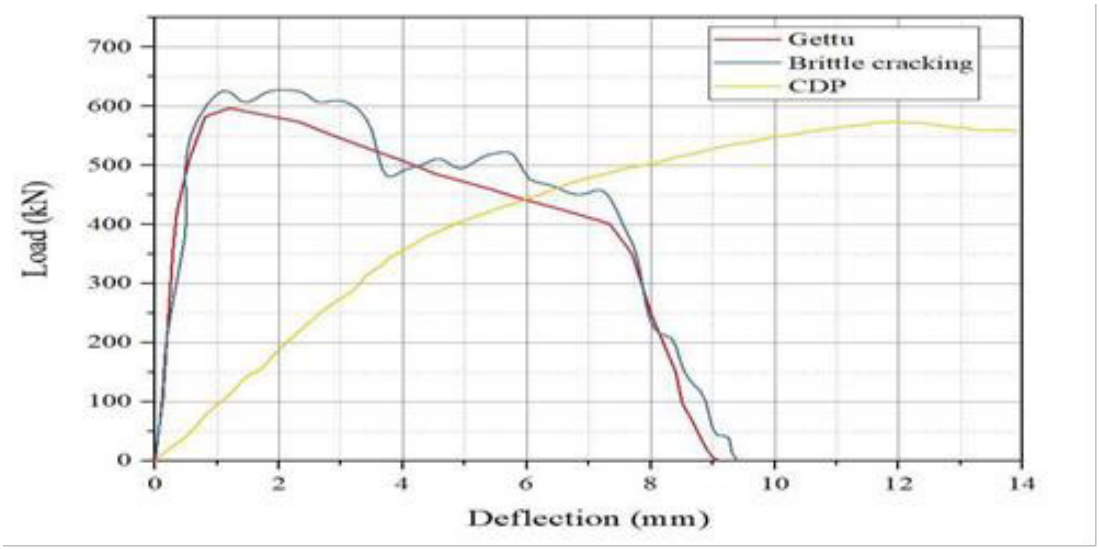

Fig. 3. Comparison of results with reference [23].

Table 2. Comparison of Reference Segment Validation Results [23].

Model type	Maximum sustained load (KN)	Maximum displacement (mm)	Percentage of maximum load error (%)	Maximum displacement error percentage (%)	Percentage of total error (%)
CDP	580	14	3	54	28.5
Brittle cracking	630	8.8	7	3	5

the continuation of the simulation, the Brittle cracking model is used to model the nonlinear part of the segment and the ring.

4- Verify

It is first necessary to simulate a ring designed with reinforcement and without fibers, and after simulating and applying geostatic loads caused by soil, to optimize the ring reinforcements used in Tehran Metro Line 7. According to Fig. 4a, the ring was created by six segments with an angle of 85.56 and a key segment with an angle of 90.18 (the ring used in the seven metro lines of Tehran). Table 3 shows the ring of Tehran Metro Line 7 by three layers of soil with different specifications. The geometric characteristics of these three soil layers are shown in Fig. 4b. To apply the loads caused by geostatic stresses of the soil in the loading part, these details are necessary and have been used in the present study.

A complete and accurate reinforcement plan is needed to simulate a ring. Hence, this study is based on the reinforcement plan of Tehran Metro Line 7. According to Fig. 5, three types of reinforcement are used as composed of transverse, longitudinal and vertical. The diameter dimensions are illustrated in Fig. 5. The distance between the longitudinal reinforcement is 100 mm, and the transverse reinforcement is 133 mm. Also, the length and width of each segment are 4350 by 1500 mm [24].

After examining the characteristics of the tunnel segment, the ring is reinforced, and the soil of Tehran Metro Line 7 is studied, which is a sample model of this research for the optimization process. Additionally, the modules expressed in this chapter were applied to simulate the Tehran Metro Line 7 ring. In the part module, the key segment and six segments were drowned first, and the reinforcements were placed in the ring. As shown in Fig. 6, the ring without the key segment was drawn, then the key segment was added to the ring. Finally, the created reinforcements were connected to the ring, and the integrated ring was formed.

In the next step, the mechanical properties of the reinforcement and concrete segments were assigned to them in the property module. In the next step, the elastic properties of reinforcement and the elasticity and plasticity of concrete were defined appropriately. As shown in Table 4, the elastic properties are given to reinforcement and concrete elements. According to the Brittle Cracking pattern, the plastic

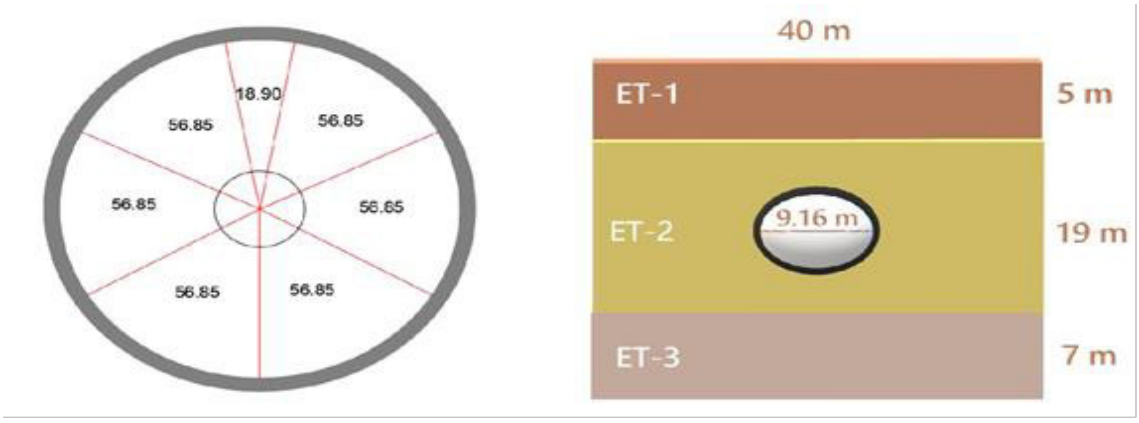

(a) (b)

Fig. 4. a) Geometric characteristics b) Soil around the ring of Tehran Metro Line 7.

Table 3. Mechanical characteristics of the soil around the ring of Tehran Metro Line 7 [24].

Soil layer number	Poisson's ratio	Young modulus (Mpa)	Internal friction angle	Cohesion (Kpa)	The soil's dry density (g/cm3)
Layer 1	0.35	35	28	31	1.70
Layer 2	0.30	75	33	15	1.84
Layer 3	0.32	50	33	30	1.90

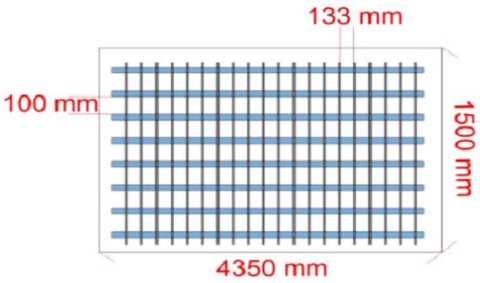

Label	No	Diameter (pp)	Length (mm)
Stirrup bar	12	16	4024
Bar	12	16	4250
Wide bar	32	10	1390

Fig. 5. Map and specifications of segment reinforcement used in Tehran Metro Line 7 [24].

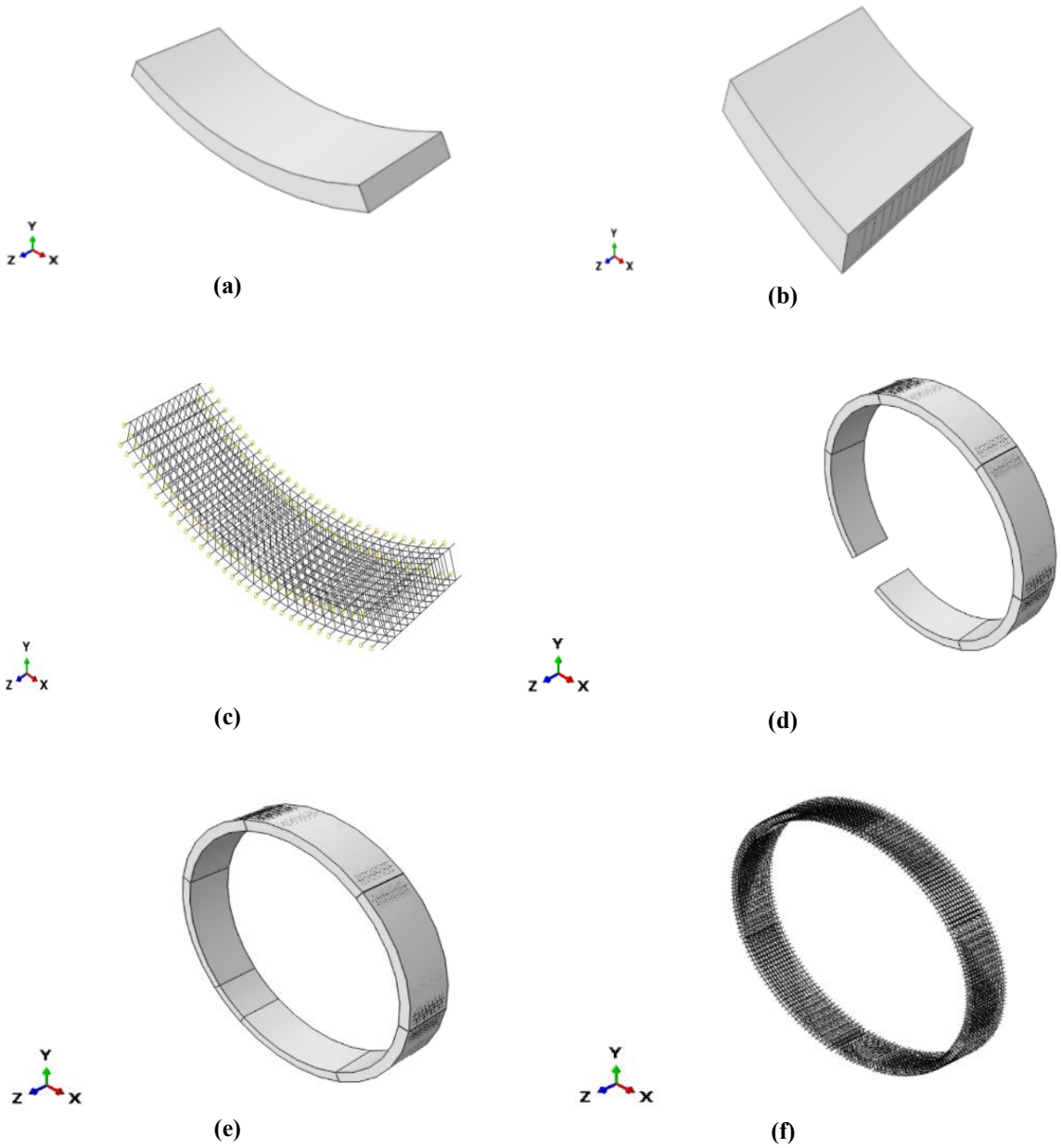

Fig. 6. Geometric drawing a) segment b) key segment c) armature segment d) ring without key e) ring armature f) ring, of Tehran metro line seven.

Table 4. Mechanical properties of concrete and ring reinforcement of Tehran Metro Line 7.

Type of Material	Young modulus (Gpa)	Poisson's ratio	density
concrete	32	0.2	2440
Armature	210	0.3	7800

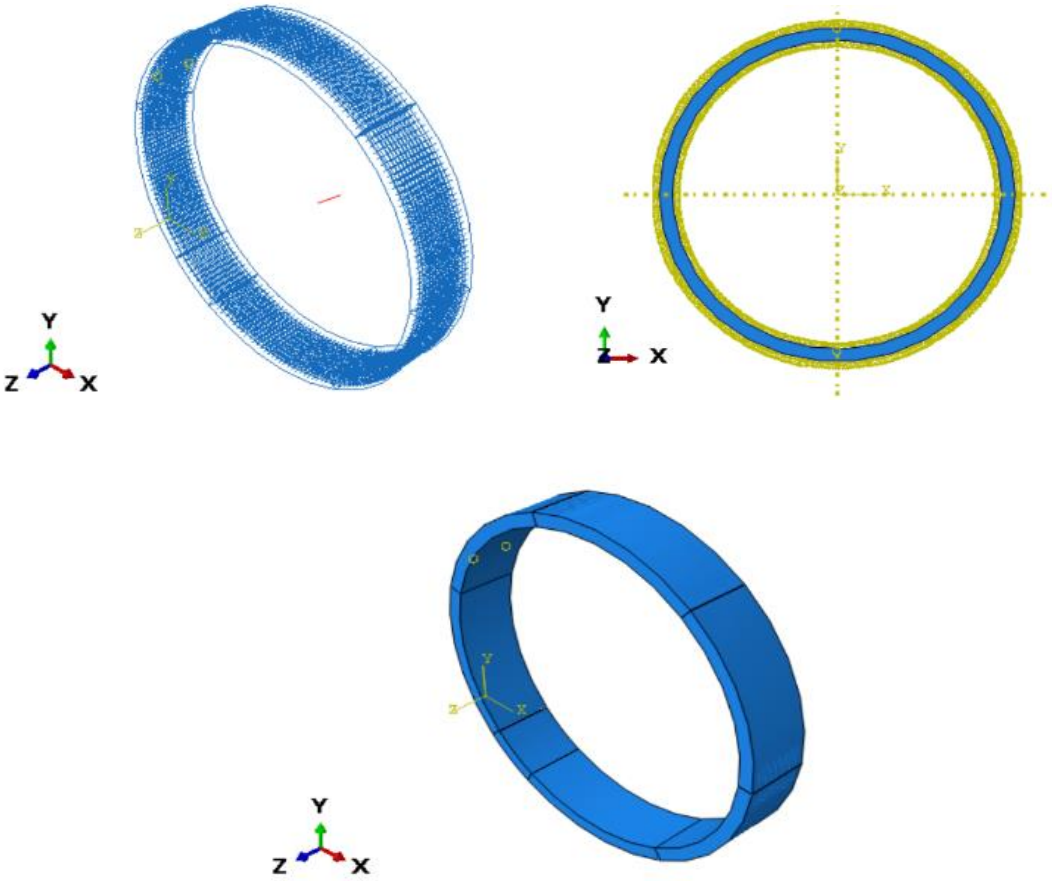

Fig. 7. Creation of internal forces between segments and reinforcement.

properties of concrete were introduced as well. According to the Merge option, the interactions of the segments with each other, as well as the interactions of the segment and the bars, were created and connected, as shown in Fig. 7.

Next, the boundary conditions and loads were created in the next step. The use of soil reaction forces is preferred over tunnel rings because very small elements were needed due to the soil simulation. Hence, no significant difference was observed in the results. Moreover, the analysis time was greatly increased, and stress concentration was observed in the elements. In this step, geostatic forces were applied to the simulated ring, which includes slag soil forces in normal and lateral forces to the body of the ring. The boundary conditions were created by ACI-544-8R, where there was another ring before and after each ring. It should be noted that the ring is not able to move in any direction and must be kept fixed with the necessary restraints of the ring. Fig. 8 shows the applied forces and boundary conditions applied to the simulated ring.

The simulated ring has meshed in the next step, after applying the boundary conditions and loading. A rectangular mesh was used due to its high efficiency with a size of 20 cm. It should be noted that the mentioned mesh size was used in the modeling because the smaller values only increase the computational run time without any change in results. An example of a mesh ring is illustrated in Fig. 9.a. After meshing and fixing possible errors, the output image of the simulated rim under the applied forces is shown, according to Fig. 9.b.

To check the accuracy of the work, the results were converted into an interaction curve and compared with the ACI-544-7R code, as shown in Fig. 10. It shows that all parts of the interaction curve are inside the interaction curve obtained from the ACI-544-7R code. Hence, the results obtained from the present study seem to be correct in terms of design.

5- Modeling

The lists of all simulated models and their characteristics in this study are compared in Table 5.

After applying the genetic algorithm, two geometric patterns of Figs. 11a & b had been selected for optimization, which was relatively resistant to the flexural loads of the primitive design. The obtained figures were compared with the proposed ACI544-7R code-optimized image in Fig. 11c.

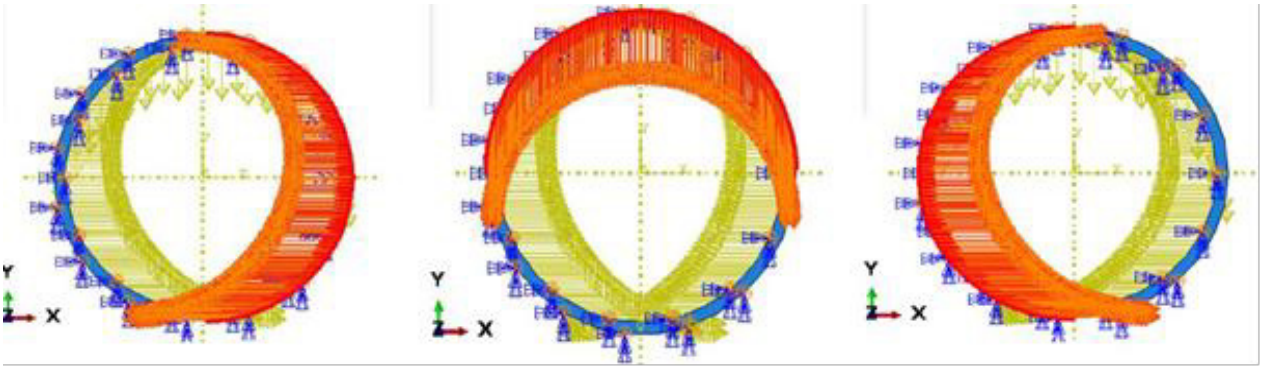

Fig. 8. Conditions and boundaries and loading of the ring.

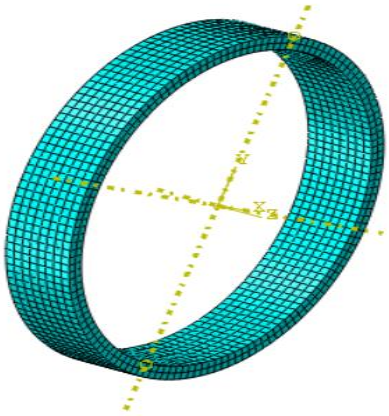

(a)

(b)

Fig. 9. a) Mesh generation b) Simulated ring output image.

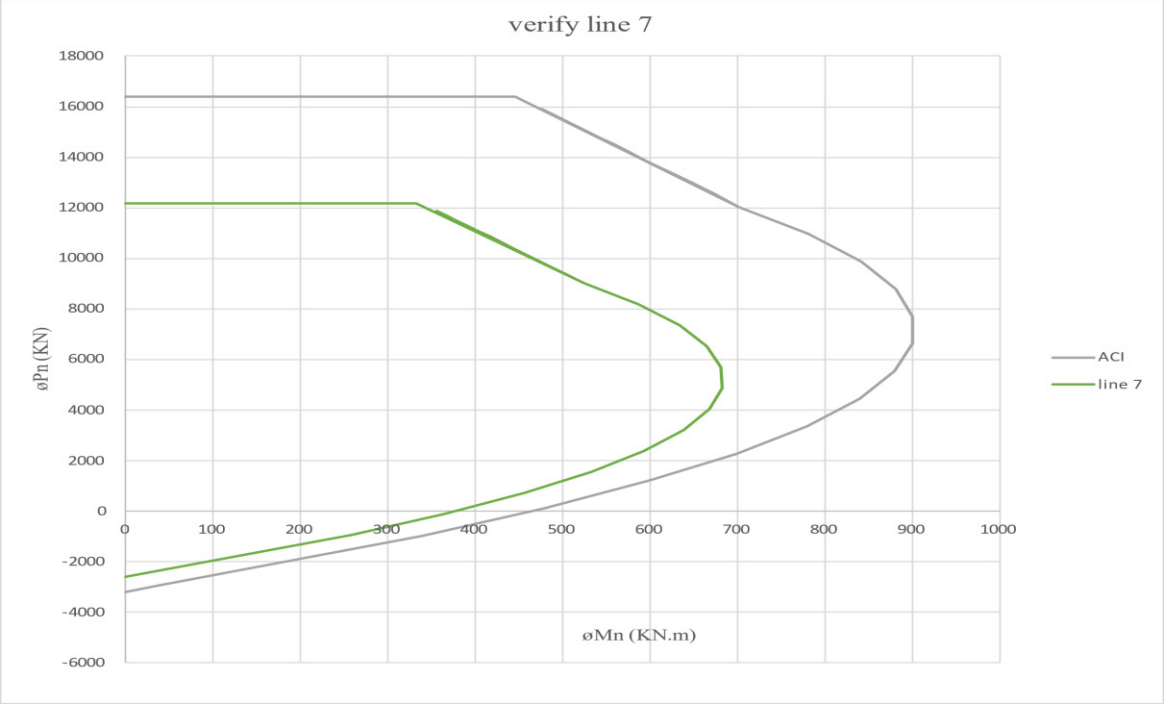

Fig. 10. Investigation of the interaction curve obtained with ACI-544-7R code.

Table 5. Simulated models.

Model type	Plastic part simulation method	Loading type	Percentage of reinforcement removed
Segment Line 9 Barcelona	CDP	Three-point bending	-
Segment Line 9 Barcelona	Brittle Cracking		-
Ring optimized by steel fibers		Geostatic stresses	%62
Ring optimized by carbon fibers			
Ring optimized by glass fibers			
Ring optimized by aramid fibers			
Ring optimized by polypropylene fibers			
Ring optimized by polypropylene and steel fibers			
segment optimized by steel fibers		Three-point bending	
segment optimized by carbon fibers			
segment optimized by glass fibers			
segment optimized by aramid fibers			
segment optimized by polypropylene fibers			
segment optimized by polypropylene and steel fibers			
whole segment reinforced completely by armature			-
plain concrete segment			-

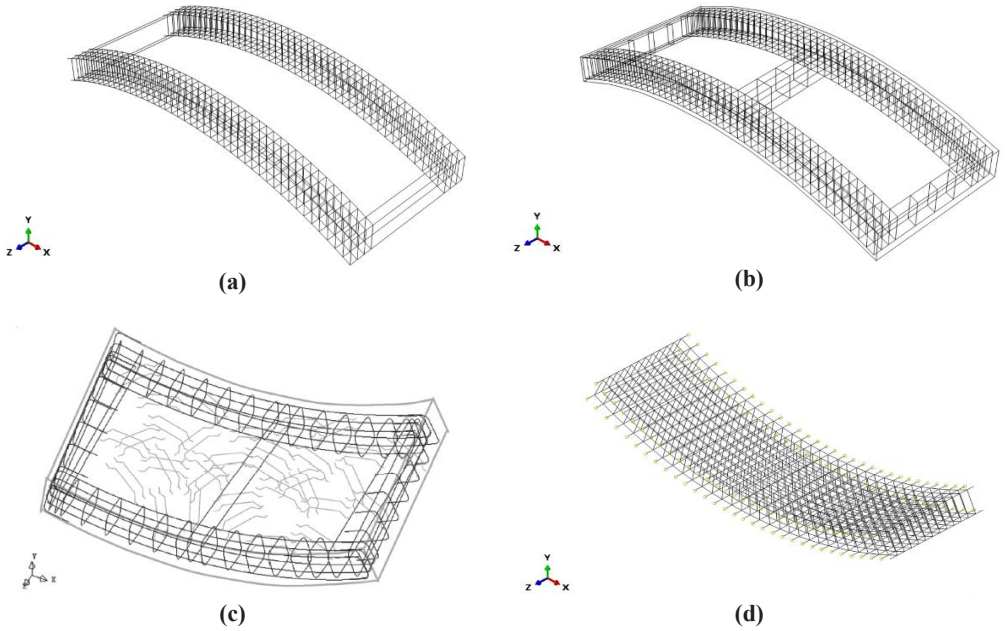

Fig. 11. Optimized geometry by fibers and a) 30% reinforcement b) 38% reinforcement c) All reinforcement d) Optimized according to ACI544-7R.

Table 6. Six optimized states of fibers used in the tunnel segment by genetic algorithm.

Type of fibers	Aramid	Steel	Glass	Carbon	Polypropylene	Combination of Steel fibers and PP
Optimal percentage	3	1	3	1.1	0/2	0.1 PP+1 Steel

As can be seen, the geometric arrangement obtained from the reinforcements is very close to the geometric shape of the ACI544-7R code. The volume percentage of reinforcement obtained in Fig. 11a is about 30%, and in Fig., 11b is about 38% of the primary segment reinforcements of all segment bars in Fig. 11d.

According to the ACI544-7R regulations, the optimized form with 38% reinforcement (although it has 8% more reinforcement than the 30% optimized form) due to its proximity to reliable authorities has been used for the next steps. It is concluded that the presence of reinforcement around the segment is necessary, and the most tensile and flexural stresses are created in the side strip of the tunnel segment, according to the obtained geometric shape and the proposed shape of ACI544-7R. In the next step, five different fibers were used in tunnel segments to resist tensile stresses. In this step, five steel, glass, aramid, carbon, and polypropylene fibers have been used to compensate for the removal effects of the reinforcement, according to applied tensile and flexural stresses. For this purpose, from zero to 3% volume fibers with 0.1% step were distributed in the segment. To compensate for the tensile stresses remaining in the tunnel segment, due to the removal of 62% of the design reinforcements, the protection against loads can be satisfied by using fibers in the tunnel segment. It should be noted that the fibers were firstly used for optimization in the genetic algorithm separately. By increasing the fibers in the convergence results, the optimal percentage was selected as appropriate data. Also, in the final step, the composition of polypropylene and steel fibers was analyzed. As illustrated in Table 6, the genetic algorithm suggests six states.

In the next step, the fibers were assigned to the ring, and the optimized geometry was used, according to Fig. 11.b. Hence, ten rings were placed next to each other, where

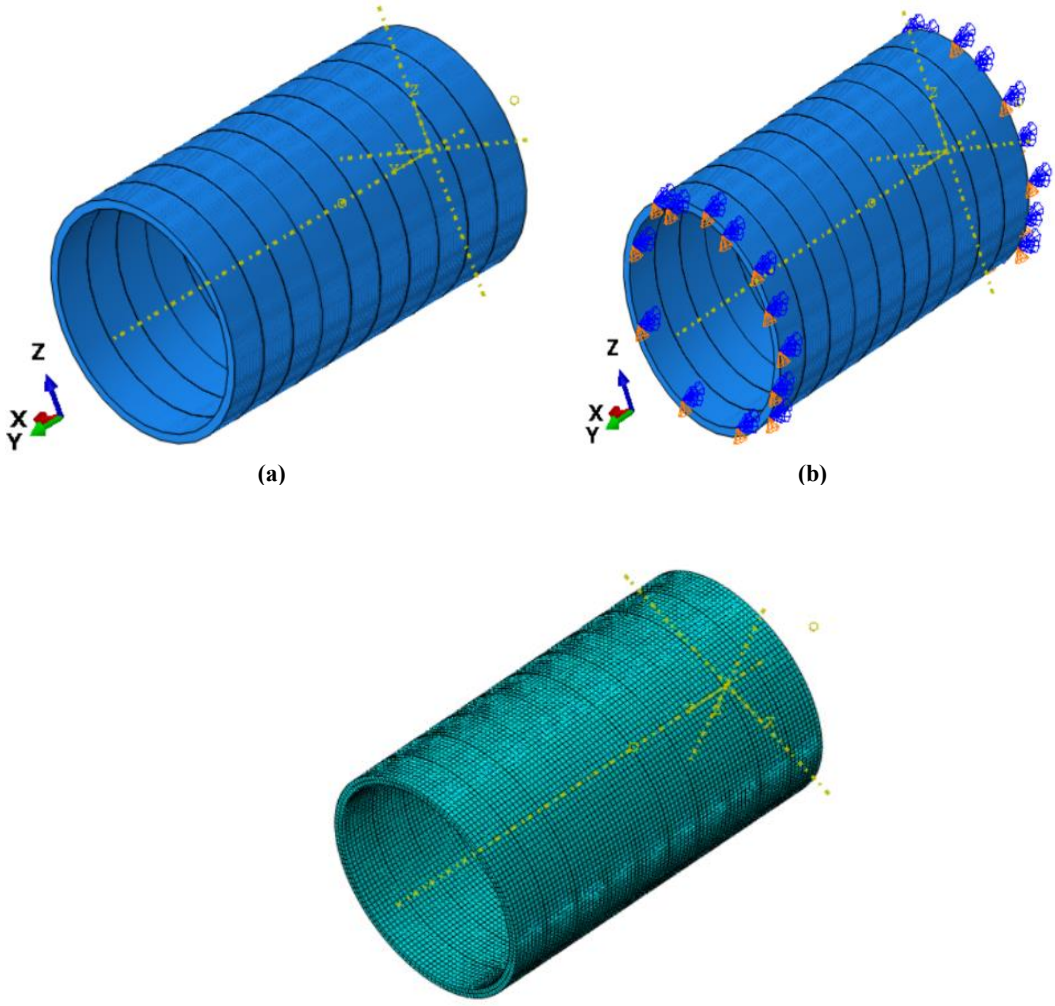

Fig. 12. a) Creating ten optimized rings with steel fibers and polypropylene b) Boundary conditions c) Mesh generation.

the created model was under the forces of soil interaction. Fig. 12.a shows the shape of the ten rings that place next to each other, which corresponds to the combination of steel fibers and polypropylene. In the created rims, the volume of reinforcements in each ring was reduced to 38% of the whole reinforcement condition due to the optimized geometry. In the next step, it is necessary to merge all the rims to connect and integrate. Then, the boundary conditions must be applied to the tunnel segment created from the ten connected rings. According to Fig. 12.b, boundary conditions were applied to the beginning and end of the tunnel, where the tunnel can properly withstand the loads caused by the soil. The load was then applied to the tunnel created from ten similarly optimized rings. After loading and boundary conditions, it is necessary to generate mesh for the created tunnel. The optimized meshing tunnel related to the combined state of steel fibers and polypropylene is shown in Fig 12.

To obtain the tunnel interaction curve, the final shape of the tunnel was obtained after correcting possible errors in ABAQUS software. It should be noted that the maximum tensile stresses were created in the areas of the tunnel where the reinforcements were present (inside the tunnel), which testifies to the correctness of the geometric optimization of the optimized segment. Also, stress concentration occurred in the beginning and end areas of the tunnel due to border conditions. Schematic images of the face and side of the optimized tunnel, related to the combined state of steel fibers and polypropylene, are shown in Fig. 13. Also, the optimized segments in all cases, such as the 2-3 section line, were simulated by a three-point bending test and compared with all reinforced concrete and non-reinforced concrete.

6- Discussions and study

It is necessary to create a tunnel interaction curve and compare it with ACI544-7R regulations. The results obtained from the numerical analysis of the ABAQUS have created a

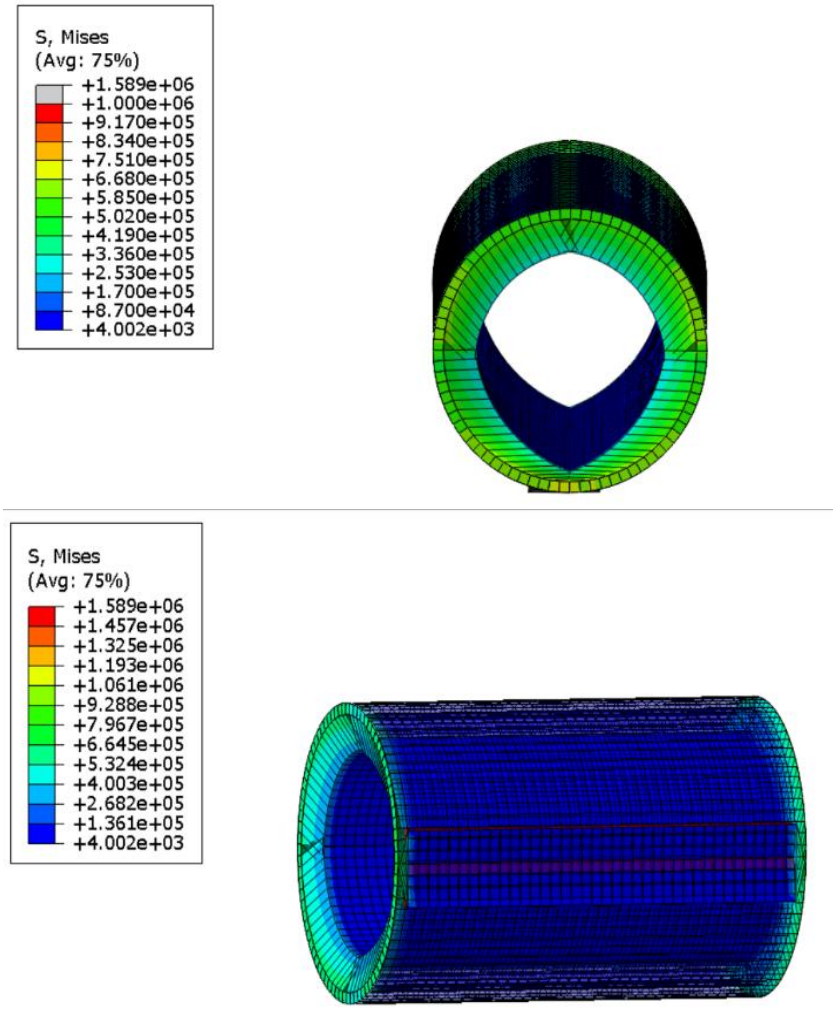

Fig. 13. Front and side view of the tunnel optimized by a combination of steel fibers and polypropylene.

tunnel interaction curve, which is compared with the ACI544-7R code in Fig. 14. As shown in Fig. 14, all optimized rings are within the safe design range compared to this regulation.

Finally, according to the validity of the force-displacement diagram, the optimized segments of steel fibers, aramid, polypropylene, carbon, glass, and a combination of polypropylene and steel fibers with designed tunnel segments of all reinforcement and unreinforced concrete under three-point bending test in the diagram of Fig. 15 were compared with each other. The optimized tunnel segment from the combination of steel and polypropylene fibers and the optimized tunnel segment from carbon fibers led to the best results, respectively.

7- Conclusion

(1) The Brittle Cracking method has closer results to the laboratory results than the CDP method.

(2) Based on the genetic algorithm, the optimized geometry was created to keep the side reinforcements along with the middle line in each segment. According to the algorithm, 62% of the segment reinforcements were removed and replaced with fibers.

(3) According to the genetic algorithm, the optimized percentage for steel, aramid, glass, carbon, and polypropylene was 1%, 3%, 3%, 1.1%, and 0.2%, respectively. Additionally, the optimized percentage for the composition of steel and polypropylene fibers was 1% and 0.1%.

(4) The interaction curve of all optimized cases (all six cases) was in the allowable range of ACI544-7R.

(5) The optimized segment with the combination of polypropylene and steel fibers showed the best response against the simulation of the three-point bending test.

(6) If two fibers separately improve the performance of the tunnel ring, their combination does not necessarily produce a better performance.

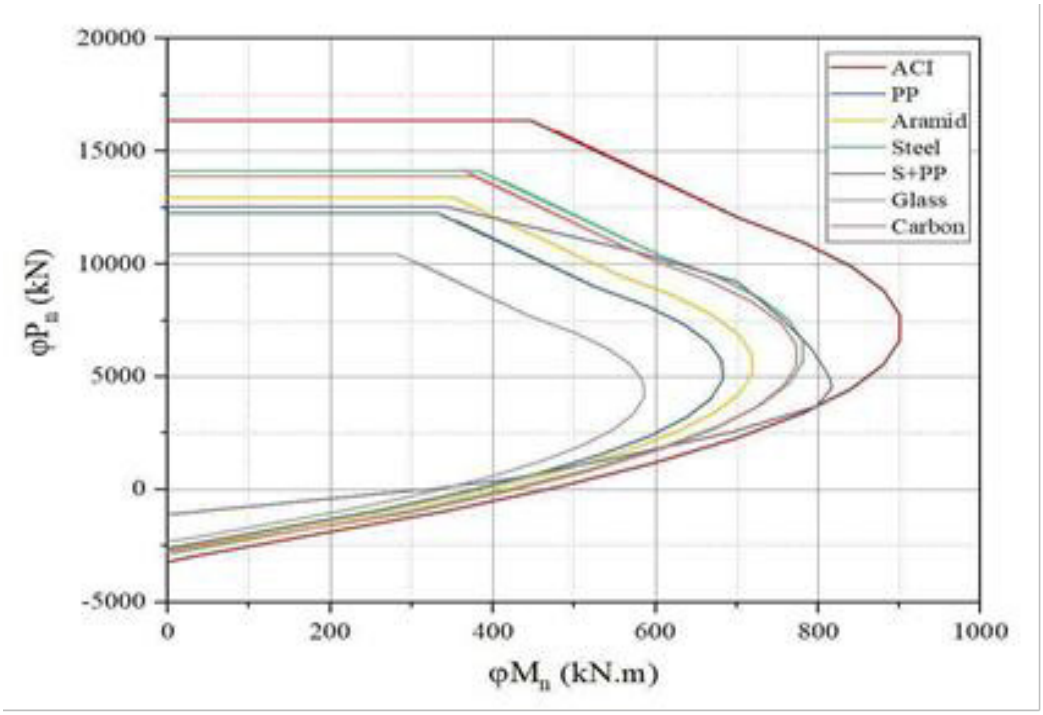

Fig. 14. Comparison of the optimized tunnel interaction curve.

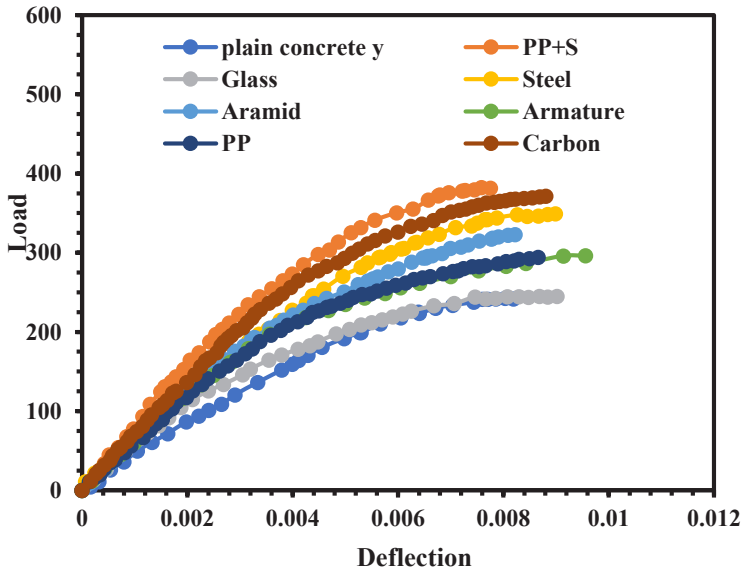

Fig. 15. Comparison of load-deflection curves of optimized segments.

References

[1] J.A. Barros, Report on design and construction of steel fiber-reinforced concrete elevated slabs, American Concrete Institute, (2015).

[2] J.A. Barros, Report on design and construction of steel fiber-reinforced concrete elevated slabs, American Concrete Institute, (2016).

[3] L. Vandewalle, D. Nemegeer, L. Balazs, B. Barr, J. Barros, P. Bartos, N. Banthia, M. Criswell, E. Denarie, M. Di Prisco, RILEM TC 162-TDF: Test and design methods for steel fibre reinforced concrete-sigma-epsilon-design method-Final Recommendation, Materials and Structures, 36(262) (2003) 560-567.

[4] M. Di Prisco, M. Colombo, D. Dozio, Fibre-reinforced concrete in fib Model Code 2010: principles, models and test validation, Structural Concrete, 14(4) (2013) 342-361.

[5] D. Moyson, Steel fibre reinforced concrete (SFRC) for tunnel linings, International Journal of Rock Mechanics and Mining Sciences and Geomechanics Abstracts, (1995), 137A.

[6] B. Chiaia, A.P. Fantilli, P. Vallini, Combining fiber-reinforced concrete with traditional reinforcement in tunnel linings, Engineering Structures, 31(7) (2009) 1600-1606.

[7] C. Molins, O. Arnau, Experimental and analytical study of the structural response of segmental tunnel linings based on an in situ loading test, Tunnelling and Underground Space Technology, 26(6) (2011) 764-777.

[8] A. De la Fuente, P. Pujadas, A. Blanco, A. Aguado, Experiences in Barcelona with the use of fibres in segmental linings, Tunnelling and Underground Space Technology, 27(1) (2012) 60-71.

[9] J. Li, H. Li, G. Ma, Y. Zhou, Assessment of underground tunnel stability to adjacent tunnel explosion, Tunnelling and Underground Space Technology, 35 (2013) 227-234.

[10] L.P. Chaves, J. Cunha, Design of carbon fiber reinforcement of concrete slabs using topology optimization, Construction and Building Materials, 73 (2014) 688-698.

[11] G. Tiberti, F. Minelli, G. Plizzari, Reinforcement optimization of fiber reinforced concrete linings for conventional tunnels, Composites Part B: Engineering, 58 (2014) 199-207.

[12] S. Koneshwaran, D.P. Blast response of segmented bored tunnel Thambiratnam, C. Gallage, using coupled SPH–FE method, Structures, 2 (2015), 58-71.

[13] A. Caratelli, A. Meda, Z. Rinaldi, S. Spagnuolo, G. Maddaluno, Optimization of GFRP reinforcement in precast segments for metro tunnel lining, Composite Structures, 181 (2017) 336-346.

[14] B. Luccioni, F. Isla, R. Codina, D. Ambrosini, R. Zerbino, G. Giaccio, M.C. Torrijos, Experimental and numerical analysis of blast response of High Strength Fiber Reinforced Concrete slabs, Engineering structures, 175 (2018) 113-122.

[15] E.A. Alwesabi, B.A. Bakar, I.M. Alshaikh, H.M. Akil, Impact resistance of plain and rubberized concrete containing steel and polypropylene hybrid fiber, Materials Today Communications, 25 (2020) 101640.

[16] O. Tengilimoglu, U. Akyuz, Experimental study on hybrid precast tunnel segments reinforced by macro-synthetic fibres and glass fibre reinforced polymer bars, Tunnelling and Underground Space Technology, 106 (2020) 103612.

[17] Z. Guo, C. Zhuang, Z. Li, Y. Chen, Mechanical properties of carbon fiber reinforced concrete (CFRC) after exposure to high temperatures, Composite Structures, 256 (2021) 113072.

[18] C. Mougeotte, P. Carlucci, S. Recchia, H. Ji, Novel approach to conducting blast load analyses using Abaqus/Explicit-CEL, ARMY ARMAMENT RESEARCH DEVELOPMENT AND ENGINEERING CENTER PICATINNY ARSENAL NJ, (2010).

[19] ASTM A820, Standard specification for steel fibers for fiber-reinforced concrete, American Society for Testing and Materials (ASTM) Committee, West Conshohocken, PA, USA, (2006).

[20] ACI 544.1 R-96, State-of-the-art report on fibre reinforced concrete, Farmington Hills, MI, USA, (2002).

[21] ASTM C1116, Standard specification for fiber-reinforced concrete and shotcrete, West Conshohocken, PA, United States, (2003).

[22] P. Hannant, Fibre cements and fibre concretes, (1978).

[23] R. Gettu, B. Barragán, T. García, G. Ramos, C. Fernández, R. Oliver, Steel fiber reinforced concrete for the Barcelona metro line 9 tunnel lining, in: Proc. of the 6th RILEM Symposium on FRC, Varenna, Italy, RILEM PRO, (2004), 141-156.

[24] M.J. Avanaki, A. Hoseini, S. Vahdani, A. de la Fuente, Numerical-aided design of fiber reinforced concrete tunnel segment joints subjected to seismic loads, Construction and Building Materials, 170 (2018) 40-54.

HOW TO CITE THIS ARTICLE

M. H. Taghavi Parsa, H. Sharifi, P. Amirchoupani, Optimization of Tunnel Reinforcements by Genetic Algorithm with the Aim of Replacing with Fibers, AUT J. Civil Eng., 6(1) (2022) 35-50.

DOI: 10.22060/ajce.2022.20088.5757